

NEUTRON FLUX CHARACTERIZATION IN TRIGA LARGE IRRADIATION CELL

James B. Tompkins and Ryan G. McClarren

Department of Nuclear Engineering
Texas A&M University, College Station, Texas, USA
tompkins@tamu.edu
rgm@tamu.edu

ABSTRACT

The one MW TRIGA reactor at Texas A&M has various methods of irradiating samples, but one of the most unique dose positions for experiments is severely underutilized. This irradiation cell is a large space where samples may be placed for activation by moving the reactor bridge to a window on the wall of the cell and operating the reactor. Due to the cell's large size, neutron flux for experiments is difficult to resolve spatially giving predictions of dose to samples a high level of uncertainty. To this end, PDT, a rapidly maturing radiation transport code, is used to simulate the neutron flux distribution for reactor experiments in the cell. To construct the PDT model, physical measurements and facility documentation are assembled, then computational methods are applied to experimental data to develop a boundary condition for neutron flux incident upon the wall shared between the reactor pool and irradiation cell. Experiments collecting neutron flux data throughout the cell are performed in an attempt to validate PDT's computational results, benefitting both the NSC and PDT development. The validation data is compared to nominal and perturbed boundary condition results with varying degrees of model complexity to determine the minimal level of computational involvement that yields results with the same degree of accuracy as more complex models. The epithermal computational predictions demonstrate the need for inclusion of higher energy groups, while the thermal model results bound almost half of the experiment data, giving confidence in the method's increased accuracy in future work.

Key Words: **Reactor Experiments, Neutron Transport, Uncertainty Quantification**

1. INTRODUCTION

The Nuclear Science Center at Texas A&M University is one of the oldest institutions with an operational research reactor, having first opened in December 1961 with continued safe and efficient operation to this day [1]. The recently renewed twenty year operation license from the Nuclear Regulatory Commission ensures that this facility will remain steadfast in its mission to advance nuclear research for years to come; however, to maintain competitive experimental capability as an irradiation facility, the NSC must be able to accurately predict sample dose and ensure these predictions consistently agree with experimental results.

Locations frequently utilized for sample irradiation are small enough that a single, volume averaged neutron flux value is sufficient to accurately predict sample dose, but some of the NSC's experimental facilities have fallen into obsolescence due to the flux distribution requiring more exhaustive studies to accurately characterize.

One such experimental location unique to the NSC is the large irradiation cell. This open space about eighteen feet by sixteen feet allows for samples of various size to be irradiated by either the NSC TRIGA reactor or a lanthanum source depending upon dose requirements for the experiment. By being one of the few nuclear research centers with facilities large enough to accommodate industrial sized equipment in a heavily irradiated environment, the NSC stands to benefit from this unique capability; so with an eye to increase experimental capacity to testing applications (e.g. electronic radiation hardening and material radiation resistance) for a broad range of samples, the facility has begun to consider the irradiation cell a potentially lucrative resource.

1.1. Problem Description

To employ the cell as an irradiation position for material testing, emissions within it must first be identified and characterized. When operating the reactor in the configuration shown in Figure 1, various forms of radiation permeate the large cell's environment, but researchers are often only interested in the dose from neutrons and/or gamma particles. In the interest of maximizing the research capability impact of this work, low energy neutrons are investigated due to their higher interaction cross sections in cell materials and effectiveness at approximating accelerated radiation damage. Low energy neutrons are fairly easy to measure when using a technique such as neutron activation analysis (NAA), but in a space so large, it would take a monumental effort to map the flux of the entire cell [2]. However, by utilizing the ease of taking flux measurements in a small area from NAA to inform a radiation transport simulation, not only would a comprehensive characterization of neutron flux within the cell be provided, but by perturbing the inputs to these simulations, a measure of uncertainty quantification can be achieved for dose throughout the cell.

From a predictive science standpoint, challenges in characterizing neutron dose in the irradiation cell include the size of the problem and numerous predictors for the quantity of interest. The cell measures approximately 484 cm long, 548 cm wide and 292 cm tall, but samples on the order of a few cubic centimeters are not uncommon in experiments in this location. How finely the simulation's mesh is divided will largely determine the efficacy of the model's flux predictions spatially thus more accurately able to provide sample dose, but higher spatial resolution also increases the degrees of freedom within

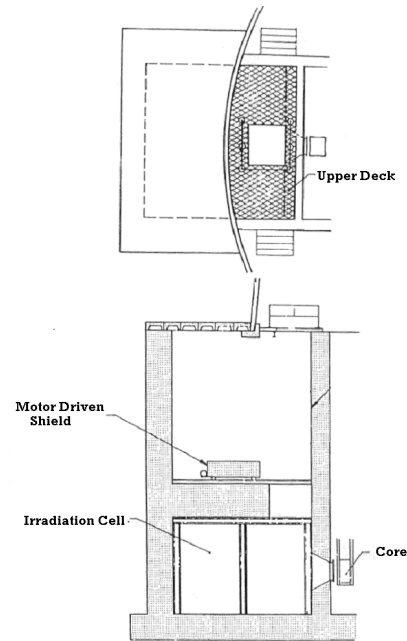


Figure 1. Top: View of the irradiation cell from above. **Bottom:** Side view of the cell.

the problem making the simulation more computationally taxing. Neutron flux will vary based on numerous parameters for this setup including positioning of the reactor, incident flux magnitude, and operational considerations (e.g. buildup of fission products such as xenon requiring higher reactivity insertion to attain a specific power). Some of these may be mitigated by consistency in experimentation such as only taking data from the first start up of the reactor every week to limit fission product buildup or ensuring the reactor bridge is locked in the same position for each experiment, but epistemic uncertainty in experiment results is witnessed by the variation of incident flux measurements under nearly identical operational conditions necessitating statistical analysis.

2. RESEARCH FOUNDATIONS

2.1. Theory and Methods

As the neutron transport simulation is used to characterize neutron flux distribution in the cell, a particular transport method must be chosen based on its applicability to the problem. One of the most commonly used deterministic conservation statements for neutron behavior in a system comes from the Boltzmann transport equation [3]

$$\frac{1}{v(E)} \frac{\partial \Phi}{\partial t} + \hat{\Omega} \cdot \nabla \Phi + \Sigma_t \Phi = \frac{\chi_p(E)}{4\pi} \int_0^\infty dE' \nu_p(E') \Sigma_f(\vec{r}, E', t) \phi(\vec{r}, E', t) + \int_{4\pi} d\hat{\Omega}' \int_0^\infty dE' \Sigma_s(\vec{r}, E') f'(\vec{r}, \hat{\Omega}' \rightarrow \hat{\Omega}, E' \rightarrow E, t) \Phi(\vec{r}, \hat{\Omega}', E', t) \quad (1)$$

presented here with each symbol having its commonly understood meaning within nuclear physics and engineering and Φ being angular flux. While simulations based on Boltzmann transport can be more computationally expensive than models relying on simplifications such as angular flux being sufficiently weakly dependent upon angle (diffusion theory), in the context of the dry cell, the angular flux on the cell's boundary is fairly forward peaked.

As with any partial differential equation, a unique solution cannot be obtained without specifying the type of system to which the solution applies, the load the system experiences, and boundary/initial conditions. Spatial parameters are determined by the cell's geometry, and material properties (specifically interaction cross sections) arise from the energy regions the study investigates in conjunction with the materials specified. With seven unique dimensional variables that must be provided as boundary conditions for transport (three in space, two in angle, one in energy, and flux magnitude), the problem is both discretized from these conditions based on mesh size, angular quadrature used, etc. and the bounds of validity for the model established (from the energy regions for which boundary conditions are provided).

The neutron activation analysis (NAA) method can determine the activity of gold-198 isotopes produced during activation of foils that include a known quantity of natural gold. Using gamma emissions

detected from the isotope, the neutron flux at the position the foil was placed is determined. The neutron activation equation (Eq. (2)) is utilized to calculate flux values from the gamma counts, foil mass, and material properties (namely gold's thermal neutron absorption cross section and resonance integral) [2]

$$N(t) = \frac{\sigma\phi N_o}{\lambda} (1 - e^{-\lambda t_{irr}}) e^{-\lambda t_{decay}}. \quad (2)$$

By using Eq. (2) with the experimental parameters of number of activated nuclei and measured activity, the scalar flux is obtained for a foil's position in the cell. Foils are thin disks about 1 cm in diameter sized such that they may be treated as point evaluations for flux wherever they are placed and are thin enough to discount attenuation and self-shielding of neutron flux.

The neutron activation technique is also useful for limiting energy bounds in the transport solution. Gold has a significant neutron absorption cross section in the thermal and epithermal energy ranges [4]. By irradiating both a bare and cadmium covered foil at the same position on the window, the magnitude of neutron flux in the epithermal and thermal regions can be determined as the cadmium will act to screen out the thermal neutrons from the gold foil it covers [4]. With one foil absorbing neutrons in both energy regions and the other only receiving epithermal dose, the thermal dose may be determined.

2.2. Experiment Equipment

To run experiments, the NSC's reactor and counting lab are employed. The reactor is a one megawatt LEU fueled pool type TRIGA fairly early in its life (refueled in 2006 with an expected lifetime of twenty-five to thirty years) [1]. The reactor is repositioned for irradiation cell operations by moving the reactor bridge along the length of the pool via a rail system. While this does introduce some ambiguity to the reactor's position in every experiment, consistent results in the flux magnitude shape on the window suggests an acceptable level of uncertainty.

Counting the foils from experiments requires the use of the NSC's High Purity Germanium detector and associated equipment and software. The HPGe is able to discriminate gamma emission energy, and a multichannel analyzer records detector counts in energy bins which CANBERRA's Genie 2000 software then performs data analysis upon to give a list of possible isotopes present in the material, the sample's activity, and associated statistics and uncertainties.

2.3. Computational Resources

Several computational resources are utilized within this study. To solve the transport equation, Texas A&M Department of Nuclear Engineering's Parallel Deterministic Transport (PDT) code is employed. PDT solves the discrete-ordinates transport problem using efficient sequential algorithms distributed in parallel [5]. PDT simulations are computed using Lawrence Livermore National Laboratory (LLNL)

computing resources through the Predictive Science Academic Alliance Program (PSAAP-II) University Partnership Program. Visualization of the flux distribution computed with PDT is performed using LLNL's VisIt graphical analysis tool [6]. A majority of the scripts created to condition experiment data for simulation input are coded in Python 2.7.9, and for various analyses including surface fitting and visualization, R is used.

3. EXPERIMENTS

Each foil's mass is measured using a high precision scale before the cadmium covered and bare foil sandwiches are prepared. The foils are then distributed in the cell or on the cell window and their positions recorded. The reactor is then positioned as close to the window as allowed and operated at one megawatt for forty-five minutes to obtain a significant dose to the foils without achieving saturation activity. Each experiment is performed on a Monday morning to mitigate the reactivity feedback effect of xenon buildup as the reactor operates throughout the week. After operation, the reactor is promptly shut down and moved to the opposite side of the pool to limit further irradiation. The foils decay for several days in the cell as activation of structural materials makes the radiological dose to personnel beyond safe occupational limits for several hours after irradiation [7]. The foils are extracted and counted on the high purity germanium detector and the activity of the foils returned is used to calculate neutron flux at the foil's position during the experiment.

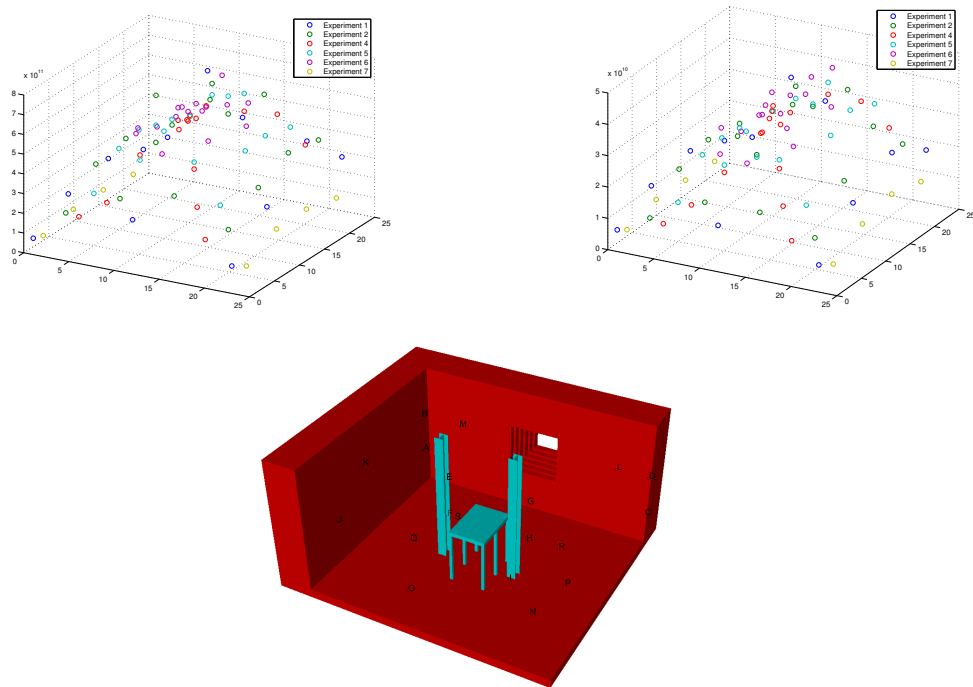


Figure 2. Left: Scatterplot of thermal flux collected on window. **Right:** Scatterplot of epithermal flux collected on window. **Bottom:** Labeled validation data collection points throughout cell.

4. SIMULATION DEVELOPMENT

4.1. Flux Magnitude Fitting

To provide flux magnitude at vertices of each cell in the mesh on the boundary of the problem, the collected window data undergoes a surface fitting technique. Several methods were explored to perform the surface fit including cubic interpolant, third order polynomial, and linear Lowess with the latter selected due to its high R^2 value, low root mean square error, and characteristic smoothed surfaces. Figure 3 illustrates the fits computed for thermal and epithermal flux groups on the cell's wall (in centimeters) shared between the reactor pool and the cell.

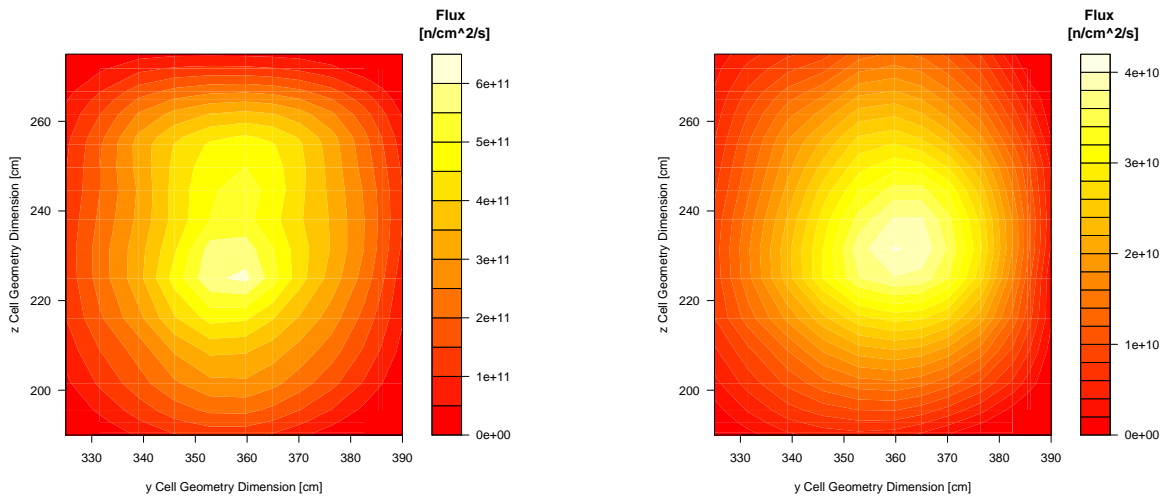


Figure 3. Left: Lowess fit of thermal flux on window. **Right:** Lowess fit of epithermal flux on window

4.2. Angular Determination

The distribution of angles on the wall of incident flux also needs to be specified for the anisotropic boundary condition. Flux measurements collected inside the cell and a point source approximation of the NSC reactor generated from an MCNP reactor model are employed for this purpose. Before determining the angular distribution, the position of the reactor relative to the irradiation cell's geometry must be determined. A Python script reads in the cell geometry by the divisions of the mesh, flux measurements, reactor point sources, and cross sections, and then a ray tracing algorithm is used to calculate expected cumulative dose at data collection points to compare to the total measured flux at those points. The reactor approximation point sources are moved throughout a region of space outside the cell that the NSC reactor can inhabit and the optimal position in relation to the irradiation cell's geometry is determined by minimizing the difference between calculated and measured scalar flux at experiment collection points.

With a reasonable approximation of the reactor's position and the flux magnitude at cell vertices, the angular flux on the boundary is calculated. A Python script takes the output from the reactor position optimization script, reactor point source data, and results from the flux fitting surfaces to compute the flux contribution at all unit vectors in the flight direction from point reactor sources and cell vertices on the wall with a flux contribution from the fit surface. Rays are traced from the reactor point sources to points on the boundary with appreciable flux contributions, and flux in that angle at the point stored. The flux at each point is normalized by the total flux through the point to determine weights for angles, then the weights assigned to angles in the chosen quadrature set. Flux for each point's angles can then be determined by the product of the angle's weight and point's flux magnitude.

5. TRANSPORT MODEL METHODS

PDT allows users to specify various spatial solution methods, geometry input, group and angle aggregation, and iterative methods for the S_N model; so for the edification of the reader, methods and options for the transport simulations produced in this study are detailed. As the large irradiation cell contains few elements that cannot be modeled in a block geometry (the irradiation window being the prime example), divisions are specified in simple three dimensional cartesian coordinates. Energy groups in the simulation have been established in Sect. 2.1: Theory & Methods, and as no upscattering is considered, both energy groups are placed in the same group set. The spatial solution method is piecewise linear discontinuous (PWLD) finite element with generalized minimal residual (GMRES) iterative method. Various angular quadrature such as linear discontinuous finite element (LDFFE) and level symmetric sets are explored with the Richardson method iterating in angle sets [8].

6. RESULTS

Nominal Results for the fully developed model are presented in Figure 4. The visualizations illustrate expected qualities of the energy region models as well as known shortcomings of the solution method. The thermal group results are diffuse throughout the cell while the higher energy epithermal region is largely dependent upon spatial and angular parameters. The streaming quality of the epithermal neutron model is much more prominent. The magnitude of the thermal region is much higher than the epithermal due to the lack of losses, higher flux on the boundary, and epithermal neutron scatters contributing to the thermal flux. Ray effects are more conspicuous in the higher energy solution as flux can vary significantly with relatively small changes in volume though they are no doubt present to some extent in the thermal region suggesting that a higher angular quadrature order is necessary for more accurate results.

While the visualizations give general qualitative impressions of the model, it will be more informative to perform a quantitative comparison of cell flux results to experiment data. The lower plots of Figure 4 detail a comparison of nominal model results at experiment collection points versus experiment flux

values. Thermal results are fairly promising, but large differences between the nominal model and experiment results typically occur closer to the irradiation window. Points A and B on the north side of the cell, close to the window are highly overestimated by the model while south wall points C and D just as close to the window are slightly underestimated. Results capture the general behavior for points E through H though are overestimated and several points (I, M, P, S) are very accurately predicted. Epithermal results are all overestimated for points closer and within view of the window (points E-H) and severely underestimated for the further out of the window's view collection points are (points A-D). Further evidence for this spatial edge underestimation can be found in points L and M. The results further away from the incident neutron boundary condition appear to have much less variance in results (points I, N-S).

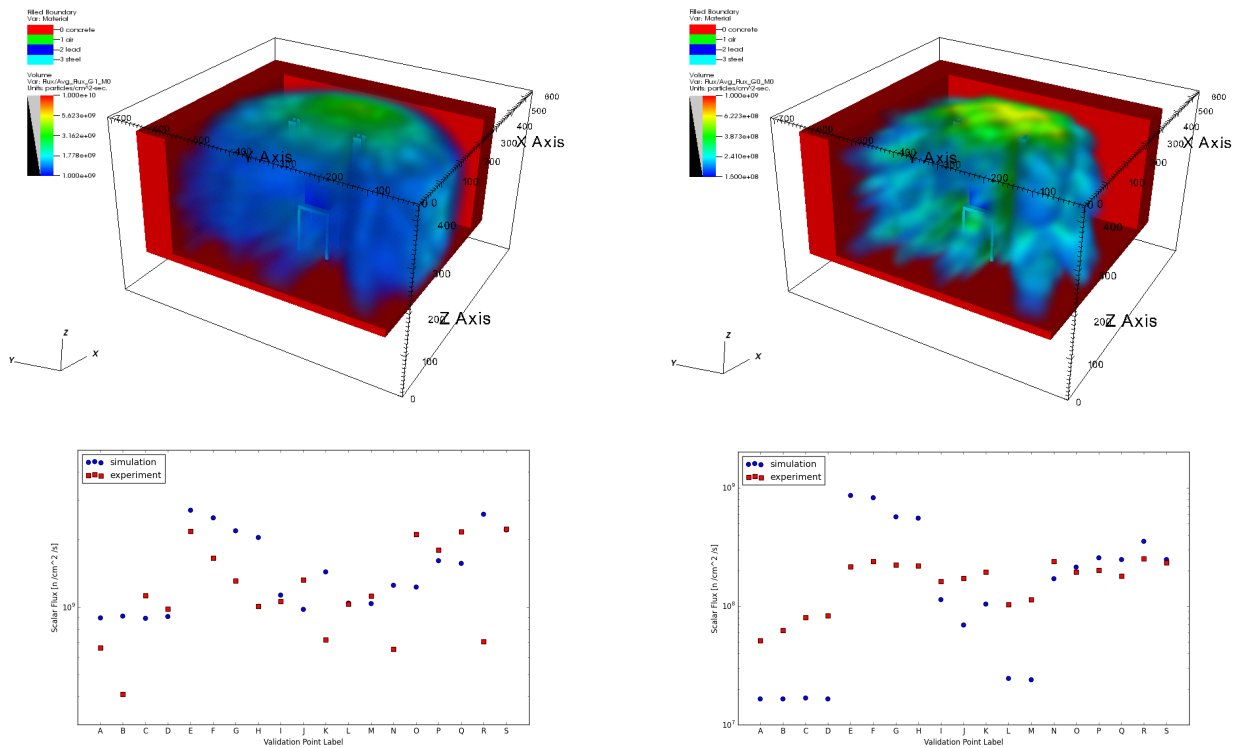


Figure 4. Nominal model results. **Top Left:** Visualization of thermal flux distribution in cell. **Top Right:** Epithermal flux distribution. **Bottom Left:** Comparison between nominal thermal flux model results and validation experiment data. **Bottom Right:** Nominal epithermal flux model results and validation data.

By perturbing the flux incident upon the cell, points where the experimental data is within realistic computational result bounds are identified. These bounded points establish where the model is predicting experimental results with a certain degree of confidence. The epithermal validation results on the right side of Figure 5 show that there are some serious problems with the model in this energy group. Only points O and S fall within the computed validation bounds and both are towards the edges of the data. The thermal validation results (left side of Figure 5) are more promising. Nine out of the nineteen data points fall within validation bounds with behaviors captured, but several are overesti-

mated including points E through H, K, N, and R and the unaccounted for lower values in two outliers (points A and B).

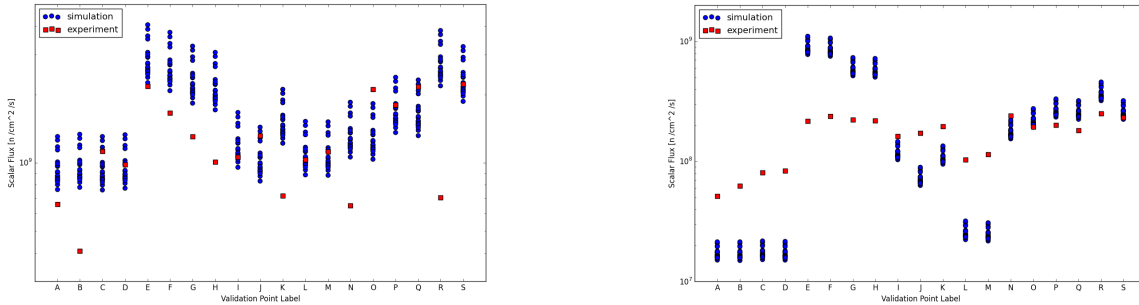


Figure 5. Perturbed Results. **Left:** Comparison between thermal flux computational bounds and validation data. **Right:** Epithermal computational bounds and validation data.

In order to determine whether some aspects of model development are necessary to accurately characterize flux in the cell, models with simpler construction are run and compared to the fully developed model’s results and experiments. The two less developed models ignore flux magnitude spatial changes on the boundary or use an isotropic angular distribution on the boundary respectively. The first uses an isotropic boundary source with the mean values of the window fits for flux magnitudes in each group across the entire wall, and the other uses the fitted flux values on the window but with angular weights equally distributed for all angles incident upon the irradiation cell’s boundary.

In the epithermal region, the isotropic mean model severely underestimates experiment data for all points. The isotropic window fit yields results disturbingly similar to the developed model. The implication that an isotropic distribution of fitted flux magnitude will work just as well as the angular distribution developed would suggest a low dependence of flux spatial distribution on incident angle of neutrons into the cell, but it is more likely that the intermediate boundary condition source is dominating the solution of these two models, making angular dependence of a lower strength source irrelevant. The isotropic model also requires specification of flux for all incident angles on the edge which increased the runtime of the simulation to around 23 minutes compared to the 7 minutes that the fully developed model requires to complete its run. These models’ trends continue in the thermal region, though the mean isotropic boundary condition predicts some points (F, G, H, K, N, and R) more accurately than the fully developed model.

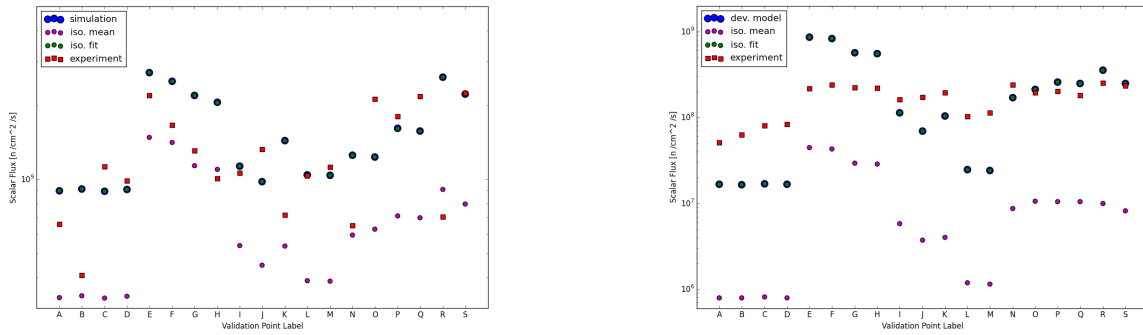


Figure 6. Model result comparisons. **Left:** Thermal model results and validation data. **Right:** Epithermal model results and validation data.

7. CONCLUSION

While the predictive capabilities of the current model are questionable, general behavior in terms of flux prediction with respect to collection points' cell position give indications of the model's spatial strengths and weaknesses. Points close to and within view of the irradiation window are typically overestimated in both energy groups, while those outside the cell window's view are severely underestimated in the epithermal range likely due to only low energy neutron flux being collected from experiments. In reality, the epithermal group neutrons will have sources throughout the cell in the form of higher energy groups' contribution as neutrons from higher energies scatter down into lower energy groups. To account for the higher energy neutrons, experiments with a greater range in energy detection bounds is necessary. The thermal flux predictions tend to be both more accurate (with nine of the experiment points agreeing with the model) and better able to predict behaviors of the experiments. In the case of points E through H, the thermal model demonstrates the negative trend evidenced in experiment data. While less than half of the experiment data agrees with the model, by collecting data through additional experiments and better calibration of boundary condition input, this first step may yield results that can be used to predict sample dose in this energy region at least.

Efforts have yielded a framework to characterize neutron flux throughout the irradiation cell, yet the model's predictive capability could undergo further refinement with the inclusion of additional considerations. To properly account for measurement error of foils from the high purity germanium activity counts, the error would need to be propagated through all points where measured flux informs the computational model as well. Starting with flux fitting, the measurement error needs to be considered along with the standard fitting error when sampling fluxes for validation. Also to be considered is the fact that the reactor's position changes slightly for every experiment. Not only will this affect the flux magnitude, but the angular distribution of flux. To account for these minute positional changes, the angular distribution of flux on the cell's boundary would need to be perturbed. The most likely way to do this would be to establish some sort of error bounds for the angular weights. The change in reactor position will also likely add more angles contributing to the flux at fitted points on the cell's east wall;

so the reactor position optimization script would need to be utilized extensively to explore which angles are possible for probable reactor locations. An obvious way to increase model accuracy is to provide better input by running more experiments to better inform model inputs. A final further consideration is that current results only use P0 scattering cross sections. A more mature study would increase the scattering level to more realistically represent downscattering from the epithermal to thermal energy regions.

REFERENCES

- [1] *Nuclear Science Center Safety Analysis Report*. Texas Engineering Experiment Station, College Station, Texas (2011).
- [2] J. E. Turner. *Atoms, Radiation, and Radiation Protection*. Wiley-VCH, Germany (2007).
- [3] G. I. Bell and S. Glasstone. *Nuclear Reactor Theory*. Robert E. Krieger Publishing Company, Malabar, FL (1970).
- [4] E. M. Baum, K. H. D., and T. R. Miller. *Nuclides and Isotopes*. Lockheed Martin Distribution Services, Cherry Hill, NJ (2002).
- [5] Parasol Algorithms and Applications Group. “Generic particle transport code.” URL <https://parasol.tamu.edu/asci/> (2012).
- [6] H. Childs *et al.* “VisIt: An End-User Tool For Visualizing and Analyzing Very Large Data.” In: *High Performance Visualization—Enabling Extreme-Scale Scientific Insight*, (pp. 357–372) (2012).
- [7] United States Regulatory Commission. “10 CFR 20.1201 Subpart C Occupational Dose Limits.” URL <http://www.nrc.gov/reading-rm/doc-collections/cfr/part020/part020-1201.html> (2010).
- [8] J. J. Jarrell and M. L. Adams. “Discrete-Ordinates Quadrature Sets Based on Linear Discontinuous Finite Elements.” URL [FullTextPDF:http://mathematicsandcomputation.cowhosting.net/MC11/_pdf/mc08_142_paper.pdf](http://mathematicsandcomputation.cowhosting.net/MC11/_pdf/mc08_142_paper.pdf) (2012).